

## Observation of the antimatter helium-4 nucleus

The STAR Collaboration\*

High-energy nuclear collisions create an energy density similar to that of the Universe microseconds after the Big Bang<sup>1</sup>; in both cases, matter and antimatter are formed with comparable abundance. However, the relatively short-lived expansion in nuclear collisions allows antimatter to decouple quickly from matter, and avoid annihilation. Thus, a high-energy accelerator of heavy nuclei provides an efficient means of producing and studying antimatter. The antimatter helium-4 nucleus ( ${}^{4}\overline{\text{He}}$ ), also known as the anti- $\alpha$  ( $\bar{\alpha}$ ), consists of two antiprotons and two antineutrons (baryon number B = -4). It has not been observed previously, although the α-particle was identified a century ago by Rutherford and is present in cosmic radiation at the ten per cent level<sup>2</sup>. Antimatter nuclei with B < -1 have been observed only as rare products of interactions at particle accelerators, where the rate of antinucleus production in high-energy collisions decreases by a factor of about 1,000 with each additional antinucleon $^{3-5}$ . Here we report the observation of  $^4\overline{\text{He}}$ , the heaviest observed antinucleus to date. In total, 18 <sup>4</sup>He counts were detected at the STAR experiment at the Relativistic Heavy Ion Collider (RHIC; ref. 6) in 10<sup>9</sup> recorded gold-on-gold (Au+Au) collisions at centre-of-mass energies of 200 GeV and 62 GeV per nucleon-nucleon pair. The yield is consistent with expectations from thermodynamic<sup>7</sup> and coalescent nucleosynthesis<sup>8</sup> models, providing an indication of the production rate of even heavier antimatter nuclei and a benchmark for possible future observations of  ${}^{4}\overline{\text{He}}$  in cosmic radiation.

In 1928, the existence of negative energy states of electrons was predicted on the basis of the application of symmetry principles to quantum mechanics, but these states were only recognised to be antimatter after the discovery of the positron (the antielectron) in cosmic radiation four years later. The predicted antiprotons and antineutrons were observed in 1955, followed by antideuterons ( $\overline{d}$ ), antitritons ( $\overline{d}$ ), and antihelium-3 ( $\overline{d}$ ) during the following two decades Recent accelerator and detector advances led to the first production of antihydrogen atoms in 1995 and the discovery of strange antimatter, the antihypertriton ( $\overline{d}$ ), in 2010 at RHIC at the Brookhaven National Laboratory (ref. 18 and references therein).

Collisions of relativistic heavy nuclei create suitable conditions for producing antinuclei, because large amounts of energy are deposited into a more extended volume 19 than that achieved in elementary particle collisions. These nuclear interactions briefly ( $\sim 10^{-23}$  s) produce hot and dense matter containing roughly equal numbers of quarks and antiquarks<sup>20</sup>, often interpreted as quark gluon plasma<sup>21</sup>. In contrast to the Big Bang, nuclear collisions produce negligible gravitational attraction and allow the plasma to expand rapidly. The hot and dense matter cools down and undergoes a transition into a hadron gas, producing nucleons and their antiparticles. The production of light antinuclei can be modelled successfully by macroscopic thermodynamics<sup>7</sup>, which assumes energy equipartition, or by a microscopic coalescence process<sup>8,22</sup>, which assumes uncorrelated probabilities for antinucleons close in position and momentum to become bound. The high temperature and high antibaryon density of relativistic heavy ion collisions provide a favourable environment for both production mechanisms.

The central detector used in our measurements of antimatter, the Time Projection Chamber  $(TPC)^{23}$  of the STAR experiment (Solenoidal

Tracker At RHIC), is situated in a solenoidal magnetic field and is used for three-dimensional imaging of the ionization trail left along the path of charged particles (Fig. 1). In addition to the momentum provided by the track curvature in the magnetic field, the detection of  $^4\overline{\text{He}}$  particles relies on two key measurements: the mean energy loss per unit track length,  $\langle \text{d}E/\text{d}x \rangle$ , in the TPC gas, which helps distinguish particles with different masses or charges, and the time of flight of particles arriving at the time of flight barrel (TOF)<sup>24</sup> surrounding the TPC. In general, time of flight provides particle identification in a higher momentum range than  $\langle \text{d}E/\text{d}x \rangle$ . The  $\langle \text{d}E/\text{d}x \rangle$  resolution is 7.5% and the timing resolution for the TOF system is 95 ps within a 7–75 ns window.

The trigger system at STAR selects collisions of interest for analysis. The minimum-bias trigger selects all particle-producing collisions, regardless of the extent of overlap of the incident nuclei. A central trigger (CENT) preferentially selects head-on collisions, rejecting about 90% of the events acquired using the minimum-bias trigger. The sample of 10<sup>9</sup> Au+Au collisions used in this search is selected on the basis of the minimum-bias trigger, on CENT, and on various specialized triggers. Preferential selection of events containing tracks with charge  $Ze = \pm 2e$  (where e is the electron charge and Z is the particle charge in units of e) was implemented using a High-Level Trigger (HLT) for data acquired in 2010. The HLT used computational resources at STAR to perform a real-time fast track reconstruction to tag events that had at least one track with a  $\langle dE/dx \rangle$  value that is larger than a threshold set to three standard deviations below the theoretically expected value<sup>25</sup> for <sup>3</sup>He at the same magnetic rigidity. The HLT successfully identified 70% of the events where a  ${}^{4}\overline{\text{He}}$  track was present while selecting only 0.4% of the events for express analyses.

Figure 2 shows  $\langle dE/dx \rangle$  versus the magnitude of magnetic rigidity, p/|Z|, where p is momentum. A distinct band of positive particles

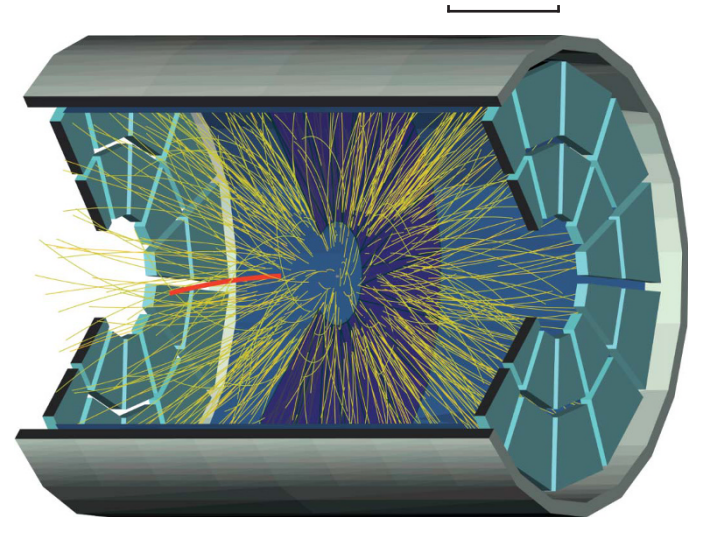


Figure 1 | A three-dimensional rendering of the STAR TPC surrounded by the TOF barrel shown as the outermost cylinder. Tracks from an event which contains a  ${}^4\overline{\text{He}}$  are shown, with the  ${}^4\overline{\text{He}}$  track highlighted in bold red.

100 cm

<sup>\*</sup>Lists of participants and their affiliations appear at the end of the paper.

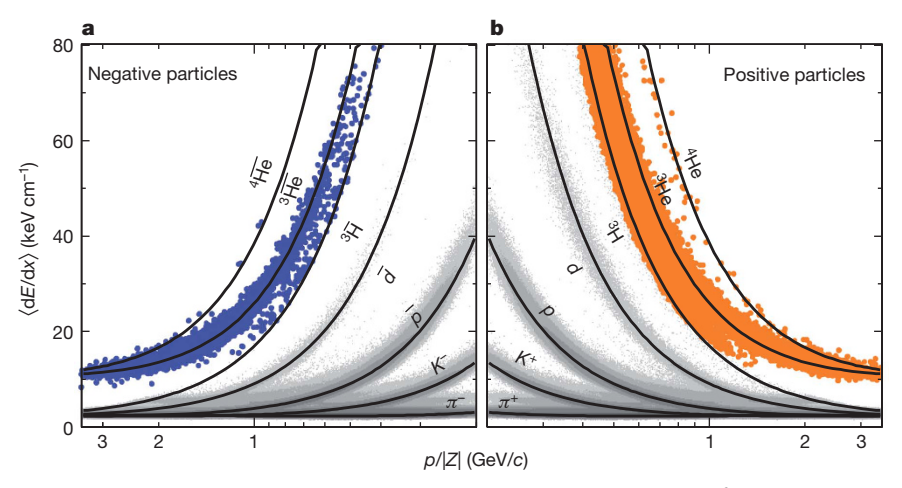


Figure 2  $|\langle dE/dx \rangle$  versus p/|Z|. a, For negatively charged particles (grey and blue dots); b, for positively charged particles (grey and orange dots). The black curves show the expected values for each species. The lower edges of the bands of coloured dots correspond to the online calculation by the HLT of  $3\sigma$  below

the  $\langle dE/dx \rangle$  band centre<sup>25</sup> for <sup>3</sup>He. The grey bands correspond to charged particles which lie far from the region of particular focus in the present study, and which were not selected by the HLT. The bands marked  $p, \bar{p}$ , K and K correspond to protons, antiprotons, kaons and pions, respectively.

centred around the expected value<sup>25</sup> for <sup>4</sup>He particles is shown in Fig. 2b and indicates that the detector is well-calibrated. In Fig. 2a, where p/|Z| is less than 1.4 GeV/c (where c is the velocity of light), four negative particles are particularly well separated from the <sup>3</sup>He band and are located within the expected band for <sup>4</sup>He. Above 1.75 GeV/c,  $\langle \mathrm{d}E/\mathrm{d}x \rangle$  values of <sup>3</sup>He and <sup>4</sup>He merge and the TOF system is needed to separate these two species.

Figure 3a and b shows the  $\langle dE/dx \rangle$  (in units of multiples of  $\sigma_{dE/dx}$ )  $n_{\sigma_{dE/dx}}$ ) versus calculated mass  $m=(p/c)\sqrt{(t^2c^2/L^2-1)}$ , where  $\sigma_{dE/dx}$  is the r.m.s. width of the  $\langle dE/dx \rangle$  distribution for  $^4He$  or  $^4\overline{He}$ , and t and L are the time of flight and path length, respectively. Negatively and positively charged particles are shown in Fig. 3a and b, respectively. In both panels, majority species are  $^3He$  and  $^3\overline{He}$ . In Fig. 3b, the  $^4He$  particles cluster around  $n_{\sigma_{dE/dx}}=0$  and mass 3.73 GeV/ $c^2$ , the appropriate mass for  $^4He$ . A similar but smaller cluster of particles can be found in Fig. 3a for  $^4\overline{He}$ . In Fig. 3c we show the projection onto the mass axis for particles in Fig. 3a and b with  $n_{\sigma_{dE/dx}}$  of -2 to 3. There is clear separation between  $^3\overline{He}$  and  $^4\overline{He}$  mass peaks. Eighteen counts for  $^4\overline{He}$  are observed. Of those, sixteen are from collisions recorded in 2010. Two counts  $^{26}$  identified by  $\langle dE/dx \rangle$  alone from data recorded in 2007 are not included in this figure, because the STAR TOF was not installed at that time.

To evaluate the background in  $^4\overline{\text{He}}$  due to  $^3\overline{\text{He}}$  contamination, we simulate the  $^3\overline{\text{He}}$  mass distribution with momenta and path lengths, as well as the expected time of flight from  $^3\overline{\text{He}}$  particles with timing resolution derived from the same data sample. The contamination from misidentifying  $^3\overline{\text{He}}$  as  $^4\overline{\text{He}}$  is estimated by integrating over the region of the  $^4\overline{\text{He}}$  selection. We estimate that the background contributes 1.4 (0.05) counts of the 15 (1) total counts from Au+Au collisions at 200 (62) GeV recorded in 2010. Therefore, the probability of misidentification is at the  $10^{-11}$  level.

The observed counts are used to calculate the antimatter yield with appropriate normalization (the differential invariant yield) in order to compare to the theoretical expectation. Detector acceptance, efficiency, and antimatter annihilation with the detector material are taken into account when computing yields. Various uncertainties related to tracking in the TPC, matching in the TOF, and triggering in the HLT are cancelled when the yield ratios of  $^4{\rm He}/^3{\rm He}$  and  $^4{\rm He}/^3{\rm He}$  are calculated. The ratios are  $^4{\rm He}/^3{\rm He}=\left(3.0\pm1.3({\rm stat})^{+0.5}_{-0.3}({\rm sys})\right)\times10^{-3}$  and  $^4{\rm He}/^3{\rm He}=\left(3.2\pm2.3({\rm stat})^{+0.7}_{-0.2}({\rm sys})\right)\times10^{-3}$  for central Au+Au collisions at 200 GeV (where 'stat' and 'sys' indicate the statistical and systematic errors). The ratios were obtained in two windows. The first was  $40^\circ < \theta < 140^\circ$ , where the polar angle,  $\theta$ , is the angle between the particle's momentum vector and the beam axis (these  $\theta$  limits correspond to limits of -1 to 1 in a related quantity, pseudorapidity). The second was a  $p_{\rm T}$  per baryon window centred at  $p_{\rm T}/$ 

 $|B|=0.875\,\mathrm{GeV/}c$  with a width of 0.25  $\mathrm{GeV/}c$ , where  $p_\mathrm{T}$  is the projection of the momentum vector on the plane that is transverse to the beam axis. Ratios calculated by a Blastwave model<sup>27</sup> for the  $p_\mathrm{T}/|B|$  window mentioned above and for the whole range of  $p_\mathrm{T}/|B|$  differ by only 1%. The differential yields (see legend to Fig. 4) for  $^4\mathrm{He}$  ( $^4\mathrm{He}$ ) are obtained by multiplying the ratio of  $^4\mathrm{He}/^3\mathrm{He}$  ( $^4\mathrm{He}/^3\mathrm{He}$ ) with the  $^3\mathrm{He}$  ( $^3\mathrm{He}$ )

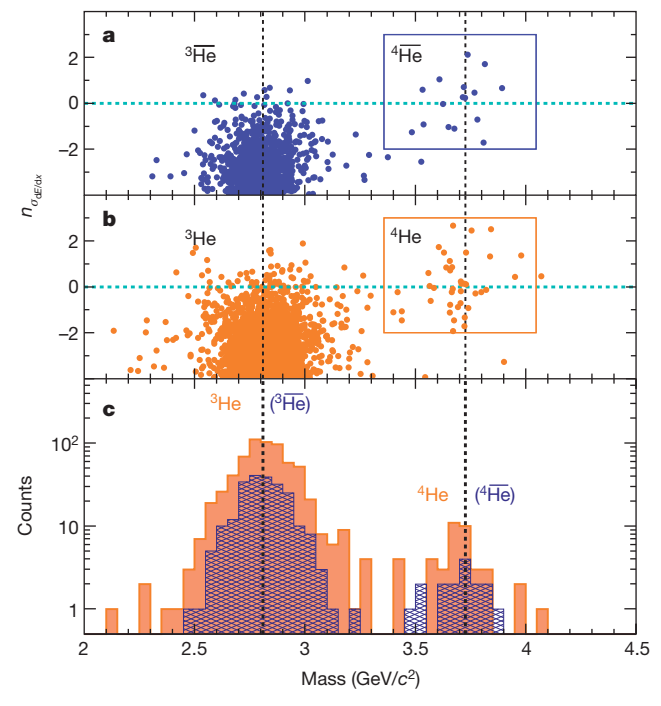


Figure 3 | Isotope identification based on energy loss and mass calculated from momentum per charge and time of flight. a, b, The  $\langle dE/dx \rangle$  in units of multiples of  $\sigma_{dE/dx}$ ,  $n_{\sigma_{dE/dx}}$ , of negatively charged particles (a) and positively charged particles (b) as a function of mass measured by the TOF system. The masses of  $^3$ He ( $^3$ He) and  $^4$ He ( $^4$ He) are indicated by the black vertical dashed lines at 2.81 GeV/ $c^2$  and 3.73 GeV/ $c^2$ , respectively. The light blue horizontal dashed line marks the position of zero deviation from the expected value of  $\langle dE/dx \rangle$  ( $n_{\sigma_{dE/dx}} = 0$ ) for  $^4$ He ( $^4$ He). The rectangular boxes highlight areas for  $^4$ He ( $^4$ He) selections:  $-2 < n_{\sigma_{dE/dx}} < 3$  and 3.35 GeV/ $c^2 <$  mass < 4.04 GeV/ $c^2$  (corresponding to a  $\pm 3\sigma$  window in mass). c, A projection of entries in a and b onto the mass axis for particles in the window of  $-2 < \sigma_{dE/dx} < 3$ . The combined measurements of energy loss and the time of flight allow a clean identification to be made in a sample of  $0.5 \times 10^{12}$  tracks from  $10^9$  Au+Au collisions.

yields²8. The systematic uncertainties consist of background (-6% for both ratios), feed-down from (anti-)hypertritons (18% for both ³He and ³He), knockouts from beam–material interactions (-5% for the ratio  $^4\text{He}/^3\text{He}$  only) and absorption (4% for the ratio  $^4\text{He}/^3\text{He}$  only). Figure 4 shows the exponential³ invariant yields versus baryon number in 200 GeV central Au+Au collisions. Empirically, the production rate reduces by a factor of  $1.6^{+1.0}_{-0.6}\times10^3\left(1.1^{+0.3}_{-0.2}\times10^3\right)$  for each additional antinucleon (nucleon) added to the antinucleus (nucleus). This general trend is expected from coalescent nucleosynthesis models³, originally developed to describe production of antideuterons²², as well as from thermodynamic models₹.

In a microscopic picture, a light nucleus emerging from a relativistic heavy-ion collision is produced during the last stage of the collision process. The quantum wavefunctions of the constituent nucleons, if close enough in momentum and coordinate space, will overlap to produce the nucleus. The production rate for a nucleus with baryon number B is proportional to the nucleon density in momentum and coordinate space, raised to the power of |B|, and therefore exhibits exponential behaviour as a function of B. Alternatively, in a thermodynamic model, a nucleus is regarded as an object with energy  $E \approx |B| m_N$ , where  $m_N$  is the nucleon mass, and the production rate is determined by the Boltzmann factor  $\exp(-E/T)$ , where T is the temperature<sup>3,7</sup>. This model also produces an exponential yield. A more rigorous calculation<sup>5</sup> can provide a good fit to the available particle yields, and predicts the ratios integrated over  $p_T$  to be  ${}^{4}\text{He}/{}^{3}\text{He} = 3.1 \times 10^{-3}$  and  ${}^{4}\overline{\text{He}}/{}^{3}\overline{\text{He}} = 2.4 \times 10^{-3}$ , consistent with our measurements. The considerations outlined above offer a good estimate for the production rate of even heavier antinuclei. For example, the yield of the stable antimatter nucleus next in line (B = -6) is predicted to be down by a factor of  $2.6 \times 10^6$  compared to  ${}^4\overline{\text{He}}$  and is beyond the reach of current accelerator technology.

A potentially more copious production mechanism for heavier antimatter is by the direct excitation of complex nuclear structures from the vacuum<sup>29</sup>. A deviation from the usual rate reduction with increasing mass would be an indication of a radically new production mechanism<sup>7</sup>. On the other hand, going beyond nuclear physics, the sensitivity of current and planned space-based charged particle detectors is below what would be needed to observe antihelium produced by nuclear interactions in the cosmos, and consequently, any observation of antihelium or even heavier antinuclei in space would indicate the

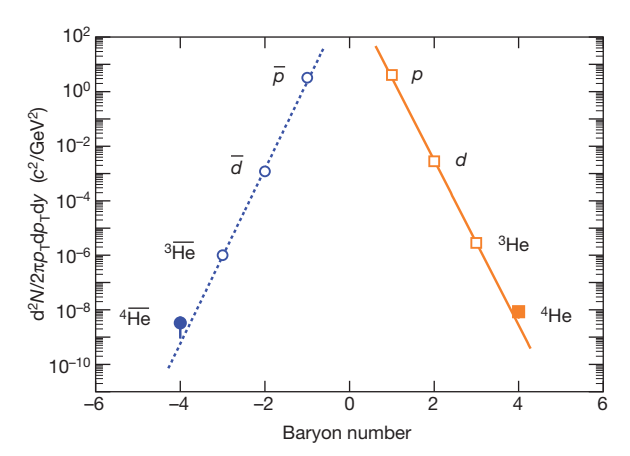


Figure 4 | Differential invariant yields as a function of baryon number, B. The differential invariant yields  $\mathrm{d}^2N/(2\pi\,p_\mathrm{T}\mathrm{d}p_\mathrm{T}\mathrm{d}y)$  were evaluated at  $p_\mathrm{T}/|B|=0.875\,\mathrm{GeV}/c$ , in central 200 GeV Au+Au collisions, where N is counts per event and y is rapidity. Yields for (anti)tritons ( $^3\mathrm{H}$  and  $^3\overline{\mathrm{H}}$ ) lie close to the positions for  $^3\mathrm{He}$  and  $^3\overline{\mathrm{He}}$ , but are not included here because of poorer identification of (anti)tritons. The lines represent fits with the exponential formula  $\propto \mathrm{e}^{-r|B|}$  for positive (solid orange line) and negative (dashed blue line) particles separately, where r is the production reduction factor. Analysis details of yields other than  $^4\mathrm{He}\,(^4\overline{\mathrm{He}})$  have been presented elsewhere  $^{4.28}$  and are plotted here as open symbols. The plotted error bars show standard statistical errors only. Systematic errors are smaller than the symbol size, and are not plotted.

existence of a large amount of antimatter elsewhere in the Universe. In particular, finding  $^4\overline{He}$  in the cosmos is one of the major motivations for space detectors such as the Alpha Magnetic Spectrometer  $^{30}$ . We have shown that  $^4\overline{He}$  exists, and have measured its rate of production in nuclear interactions, providing a point of reference for possible future observations in cosmic radiation. Barring one of those dramatic discoveries mentioned above or a new breakthrough in accelerator technology, it is likely that  $^4\overline{He}$  will remain the heaviest stable antimatter nucleus observed for the foreseeable future.

## Received 14 March; accepted 4 April 2011. Published online 24 April 2011.

- Lemaître, G. A homogeneous universe of constant mass and increasing radius accounting for the radial velocity of extragalactic nebulae [in French]. Ann. Soc. Sci. Brux. 47, 49–55 (1927).
- Wiebel-Sooth, B., Biermann, P. & Meyer, H. Cosmic rays, VII. Individual element spectra: prediction and data. Astron. Astrophys. 330, 389–398 (1998).
- Armstrong, T. A. et al. Mass dependence of light-nucleus production in ultrarelativistic heavy-ion collisions. Phys. Rev. Lett. 83, 5431–5434 (1999).
- Liu, H. Production of Meson, Baryon and Light Nuclei (A=2,3): Investigating Freeze-Out Dynamics and Roles of Energetic Quarks and Gluons in Au+Au Collisions at RHIC. PhD thesis, Univ. Sci. Technol. China (2007).
- Andronic, Á., Braun-Munzinger, P., Stàchel, J. & Stöcker, H. Production of light nuclei, hypernuclei and their antiparticles in relativistic nuclear collisions. *Phys. Lett. B* 697, 203–207 (2011).
- Harrison, M., Ludlam, T. & Ozaki, S. The relativistic heavy ion collider project: RHIC and its detectors. Nucl. Instrum. Methods Phys. Res. A 499, 235–244 (2003).
- Braun-Munzinger, P. & Stachel, J. The quest for the quark-gluon plasma. Nature 448, 302–309 (2007).
- Sato, H. & Yazaki, K. On the coalescence model for high energy nuclear reactions. Phys. Lett. B 98, 153–157 (1981).
- Dirac, P. A. M. The quantum theory of the electron. Proc. R. Soc. Lond. A 117, 610–624 (1928).
- 10. Anderson, C. D. The positive electron. Phys. Rev. 43, 491-494 (1933).
- Chamberlain, O., Segrè, E., Wiegand, C. & Ypsilantis, T. Observation of antiprotons. Phys. Rev. 100, 947–950 (1955).
- Cork, B., Lambertson, G. R., Piccioni, O. & Wenzel, W. A. Antineutrons produced from antiprotons in charge-exchange collisions. *Phys. Rev.* **104**, 1193–1197 (1956).
- Massam, T., Muller, T., Righini, B., Schneegans, M. & Zichichi, A. Experimental observation of antideuteron production. *Nuovo Cim.* 39, 10–14 (1965).
- Dorfan, D. E., Eades, J., Lederman, L. M., Lee, W. & Ting, C. C. Observation of antideuterons. *Phys. Rev. Lett.* 14, 1003–1006 (1965).
- Vishnevsky, N. K. et al. Observation of antitritium [in Russian]. Yad. Fiz. 20, 694–708 (1974).
- Antipov, Y. M. et al. Observation of antihelium3 [in Russian]. Yad. Fiz. 12, 311–322 (1970)
- 17. Baur, G. et al. Production of antihydrogen. Phys. Lett. B 368, 251–258 (1996).
- Abelev, B. I. et al. Observation of an antimatter hypernucleus. Science 328, 58–62 (2010).
- Lee, T. D. Abnormal nuclear states and vacuum excitation. Rev. Mod. Phys. 47, 267–275 (1975).
- BRAHMS, PHENIX, PHOBOS, and STAR Collaboration. RHIC white papers. Nucl. Phys. A 757, Issues 1–2, 1–283 (2005).
- Heinz, U., Subramanian, P. R., Stöcker, H. & Greiner, W. Formation of antimatter clusters in the hadronization phase transition. J. Phys. G 12, 1237–1263 (1986).
- Butler, S. T. & Pearson, C. A. Deuterons from high-energy proton bombardment of matter. *Phys. Rev. Lett.* 7, 69–71 (1961).
- Anderson, M. et al. The STAR time projection chamber: a unique tool for studying high multiplicity events at RHIC. Nucl. Instrum. Methods Phys. Res. A 499, 659–678 (2003).
- Bonner, B. et al. A single time-of-flight tray based on multigap resistive plate chambers for the STAR experiment at RHIC. Nucl. Instrum. Methods Phys. Res. A 508, 181–184 (2003).
- Bichsel, H. A method to improve tracking and particle identification in TPCs and silicon detectors. Nucl. Instrum. Methods Phys. Res. A 562, 154–197 (2006).
- Zhou, J. Light (Anti)Nuclei Production in the STAR Experiment at RHIC. Ph.D. thesis, Rice Univ. (2009).
- Tang, Z. et al. Spectra and radial flow in relativistic heavy ion collisions with Tsallis statistics in a blast-wave description. Phys. Rev. C 79, 051901(R) (2009).
- 28. Abelev, B. I. *et al.*, STAR Collaboration. Yields and elliptic flow of *d* (d) and <sup>3</sup>He (<sup>3</sup>He) in Au + Au collisions at  $\sqrt{s_{NN}} = 200$  GeV. Preprint at (http://arxiv.org/abs/0909.0566) (2009).
- 29. Greiner, W. On the extension of the periodic system into the sectors of strangeness and antimatter. *Int. J. Mod. Phys. E* **5**, 1–90 (1996).
- Ahlen, S. et al. An antimatter spectrometer in space. Nucl. Instrum. Methods Phys. Res. A 350, 351–367 (1994).

Acknowledgements We thank the RHIC Operations Group and RACF at BNL, the NERSC Center at LBNL and the Open Science Grid consortium for providing resources and support. This work was supported in part by the Offices of NP and HEP within the US DOE Office of Science, the US NSF, the Sloan Foundation, the DFG cluster of excellence 'Origin and Structure of the Universe' of Germany, CNRS/IN2P3, FAPESP



CNPq of Brazil, the Ministry of Education and Science of the Russian Federation, NNSFC, CAS, MoST and MoE of China, GA and MSMT of the Czech Republic, FOM and NWO of the Netherlands, DAE, DST and CSIR of India, the Polish Ministry of Science and Higher Education, the Korea Research Foundation, the Ministry of Science, Education and Sports of Croatia, and RosAtom of Russia.

Author Contributions All authors contributed equally.

Author Information Reprints and permissions information is available at www.nature.com/reprints. The authors declare no competing financial interests. Readers are welcome to comment on the online version of this article at www.nature.com/nature. Correspondence and requests for materials should be addressed to The Star Collaboration (star-antihe4-I@lists.bnl.gov).

#### The STAR Collaboration

The STAR Collaboration

H. Agakishiev<sup>1</sup>, M. M. Aggarwal<sup>2</sup>, Z. Ahammed<sup>3</sup>, A. V. Alakhverdyants<sup>1</sup>, I. Alekseev<sup>4</sup>, J. Alford<sup>5</sup>, B. D. Anderson<sup>5</sup>, C. D. Anson<sup>6</sup>, D. Arkhipkin<sup>7</sup>, G. S. Averichev<sup>1</sup>, J. Balewski<sup>8</sup>, D. R. Beavis<sup>2</sup>, N. K. Behers<sup>3</sup>, R. Bellwied<sup>10</sup>, M. J. Betancourt<sup>8</sup>, R. R. Betts<sup>11</sup>, A. Bhasin<sup>12</sup>, A. K. Bhati<sup>2</sup>, H. Bichsel<sup>13</sup>, J. Bielcikous<sup>15</sup>, B. Biritz<sup>16</sup>, L. C. Bland<sup>7</sup>, I. G. Bordyuzhin<sup>4</sup>, W. Borowski<sup>17</sup>, J. Bouchet<sup>5</sup>, E. Braidot<sup>18</sup>, A. V. Brandin<sup>19</sup>, A. Bridgeman<sup>20</sup>, S. G. Brovko<sup>21</sup>, E. Bruna<sup>22</sup>, S. Bueltmann<sup>23</sup>, I. Bunzarov<sup>1</sup>, T. P. Burton<sup>7</sup>, X. Z. Cai<sup>24</sup>, H. Caines<sup>22</sup>, M. Calderon<sup>21</sup>, D. Cebra<sup>21</sup>, R. Cendejas<sup>16</sup>, M. C. Cervantes<sup>25</sup>, Z. Chajecki<sup>6</sup>, P. Chang<sup>25</sup>, M. Charloyadhyay<sup>26</sup>, H. F. Chen<sup>27</sup>, J. H. Chen<sup>24</sup>, J. Y. Chen<sup>28</sup>, L. Chen<sup>28</sup>, J. Cheng<sup>29</sup>, M. Cherney<sup>30</sup>, A. Chikanian<sup>22</sup>, K. E. Choi<sup>31</sup>, W. Christie<sup>7</sup>, P. Chung<sup>15</sup>, M. J. M. Codrington<sup>25</sup>, R. Corliss<sup>8</sup>, J. G. Cramer<sup>13</sup>, H. J. Crawford<sup>32</sup>, A. Davila Leyva<sup>33</sup>, L. C. De Silva<sup>10</sup>, R. R. Debbe<sup>7</sup>, T. G. Dedovich<sup>1</sup>, A. A. Derevschikov<sup>34</sup>, R. Derradi de Souza<sup>35</sup>, L. Didenko<sup>7</sup>, P. Djawotho<sup>25</sup>, S. M. Dogra<sup>12</sup>, X. Dong<sup>3</sup>, J. L. Drachenberg<sup>25</sup>, J. E. Draper<sup>21</sup>, J. C. Dunlop<sup>7</sup>, L. G. Efirnov<sup>1</sup>, M. Enimin<sup>36</sup>, J. Engelaga<sup>32</sup>, G. Eppley<sup>37</sup>, M. Estienne<sup>7</sup>, L. Elun<sup>38</sup>, O. Evdokimov<sup>11</sup>, R. Fatemii<sup>39</sup>, J. Fedorisin<sup>1</sup>, R. G. Fersch<sup>39</sup>, P. Filip<sup>1</sup>, E. Finch<sup>2</sup>, V. Fine<sup>7</sup>, Y. Fisyak<sup>7</sup>, C. A. Gagliardi<sup>25</sup>, D. R. Gangadharan<sup>16</sup>, F. Geurts<sup>37</sup>, P. Ghosh<sup>26</sup>, Y. N. Gorbunov<sup>30</sup>, A. Gordon<sup>7</sup>, O. G. Grebenyuk<sup>3</sup>, D. Grosnick<sup>40</sup>, S. M. Guertin<sup>16</sup>, A. Gupta<sup>12</sup>, S. Gupta<sup>12</sup>, W. Guryn<sup>7</sup>, B. Haag<sup>21</sup>, O. Hajkova<sup>14</sup>, A. Hamed<sup>25</sup>, L. X. Han<sup>24</sup>, J. W. Harris<sup>22</sup>, J. P. Hays-Wehle<sup>8</sup>, M. Heinz<sup>22</sup>, S. Heppelmann<sup>38</sup>, A. Hirsch<sup>41</sup>, E. Hjort<sup>3</sup>, G. W. Hoffmann<sup>3</sup>, D. J. Hofman<sup>11</sup>, B. Huang<sup>27</sup>, H. Z. Huang<sup>16</sup>, T. J. Humanic<sup>6</sup>, L. Huo<sup>25</sup>, G. Igo<sup>16</sup>, P. Jacobs<sup>3</sup>, W. W. Jacobs<sup>42</sup>, J. Koralet<sup>31</sup>, J. Soeph<sup>5</sup>, E. G. Judd<sup>32</sup>, S. Kabana<sup>17</sup>, K. Kang<sup>29</sup>, J. Korles<sup>3</sup>, J. Soeph<sup>5</sup>, E. G.

Scharenberg<sup>41</sup>, A. M. Schmah<sup>3</sup>, N. Schmitz<sup>51</sup>, T. R. Schuster<sup>45</sup>, J. Seele<sup>8</sup>, J. Seger<sup>30</sup>, I. Selyuzhenkov<sup>42</sup>, P. Seyboth<sup>51</sup>, N. Shah<sup>16</sup>, E. Shahaliev<sup>1</sup>, M. Shao<sup>27</sup>, M. Sharma<sup>36</sup>, S. S. Shi<sup>28</sup>, Q. Y. Shou<sup>24</sup>, E. P. Sichtermann<sup>3</sup>, F. Simon<sup>51</sup>, R. N. Singaraju<sup>26</sup>, M. J. Skoby<sup>41</sup>, N. Smirnov<sup>22</sup>, D. Solanki<sup>50</sup>, P. Sorensen<sup>7</sup>, H. M. Spinka<sup>20</sup>, B. Srivastava<sup>41</sup>, T. D. S. Stanislaus<sup>40</sup>, D. Staszak<sup>16</sup>, S. G. Steadman<sup>8</sup>, J. R. Stevens<sup>42</sup>, R. Stock<sup>45</sup>, M. Strikhanov<sup>19</sup>, B. Stringfellow<sup>41</sup>, A. A. P. Suaide<sup>47</sup>, M. C. Suarez<sup>11</sup>, N. L. Subba<sup>5</sup>, M. Sumbera<sup>15</sup>, X. M. Sun<sup>3</sup>, Y. Sun<sup>27</sup>, Z. Sun<sup>49</sup>, B. Surrow<sup>8</sup>, D. N. Svirida<sup>4</sup>, T. J. M. Symons<sup>3</sup>, A. Szanto de Toledd<sup>47</sup>, J. Takahashi<sup>35</sup>, A. H. Tang<sup>7</sup>, Z. Tang<sup>27</sup>, L. H. Tarnini<sup>36</sup>, T. Tarnowsky<sup>52</sup>, D. Thein<sup>33</sup>, J. H. Thomas<sup>3</sup>, J. Tian<sup>24</sup>, A. R. Timmins<sup>10</sup>, D. Tlusty<sup>15</sup>, M. Tokarev<sup>1</sup>, T. A. Trainor<sup>13</sup>, S. Trentalange<sup>16</sup>, R. E. Tribble<sup>25</sup>, P. Tribedy<sup>26</sup>, O. D. Tsai<sup>16</sup>, T. Ullrich<sup>7</sup>, D. G. Underwood<sup>20</sup>, G. Van Buren<sup>7</sup>, G. van Nieuwenhuizen<sup>8</sup>, J. A. Vanfossen Jr<sup>5</sup>, R. Varma<sup>9</sup>, G. M. S. Vasconcelos<sup>35</sup>, A. N. Vasiliev<sup>34</sup>, F. Videbaek<sup>7</sup>, Y. P. Viyogi<sup>26</sup>, S. Vokal<sup>1</sup>, S. A. Voloshin<sup>36</sup>, M. Wada<sup>33</sup>, M. Walker<sup>8</sup>, F. Wang<sup>41</sup>, G. Wang<sup>16</sup>, H. Wang<sup>52</sup>, J. S. Wang<sup>49</sup>, Q. Wang<sup>41</sup>, X. L. Wang<sup>27</sup>, Y. Wang<sup>29</sup>, G. Webb<sup>39</sup>, J. C. Webb<sup>7</sup>, G. D. Westfall<sup>52</sup>, C. Whitten Jr<sup>16</sup>\*, H. Wieman<sup>3</sup>, S. W. Wissink<sup>42</sup>, R. Witt<sup>53</sup>, W. Witzke<sup>39</sup>, Y. F. Wu<sup>28</sup>, Z. Xiao<sup>29</sup>, W. Xie<sup>41</sup>, H. Xu<sup>49</sup>, N. Xu<sup>32</sup>, Q. H. Xu<sup>46</sup>, W. Xu<sup>16</sup>, Y. Xu<sup>27</sup>, Z. Xu<sup>7</sup>, L. Xue<sup>24</sup>, Y. Yang<sup>28</sup>, P. Yepes<sup>37</sup>, K. Yigh, J. F. P. Lang<sup>29</sup>, Y. P. Lan

<sup>1</sup> Joint Institute for Nuclear Research, Dubna, 141 980, Russia. <sup>2</sup> Panjab University, Chandigarh 160014. India, <sup>3</sup>Lawrence Berkeley National Laboratory, Berkeley, California 94720, USA. <sup>4</sup>Alikhanov Institute for Theoretical and Experimental Physics, Moscow 117218, Russia. <sup>5</sup>Kent State University, Kent, Ohio 44242, USA. <sup>6</sup>Ohio State University, Columbus, Ohio 43210, USA. <sup>7</sup>Brookhaven National Laboratory, Upton, New York 11973, USA. <sup>8</sup>Massachusetts Institute of Technology, Cambridge, Massachusetts 02139-4307, USA. <sup>9</sup>Indian Institute of Technology, Mumbai 400076, India. <sup>10</sup>University of Houston, Houston, Texas 77204, USA. <sup>11</sup>University of Illinois at Chicago, Chicago, Illinois 60607, USA. <sup>12</sup>University of Jammu, Jammu 180001, India. <sup>13</sup>University of Washington, Seattle, Washington 98195, USA. <sup>14</sup>Czech Technical University in Prague, FNSPE, Prague, 115 19, Czech Republic. <sup>15</sup>Nuclear Physics Institute AS CR, 250 68 Řež/Prague, Czech Republic. <sup>16</sup>University of California, Los Angeles, California 90095, USA. <sup>17</sup>SUBATECH, Nantes 44307, France. <sup>18</sup>NIKHEF and Utrecht University, Amsterdam 1098 XG, The Netherlands. 44307, France. <sup>19</sup>NIKHEF and Utrecht University, Amsterdam 1098 XG, The Netherlands. <sup>19</sup>Moscow Engineering Physics Institute, Moscow 115409, Russia. <sup>20</sup>Argonne National Laboratory, Argonne, Illinois 60439, USA. <sup>21</sup>University of California, Davis, California 95616, USA. <sup>22</sup>Yale University, New Haven, Connecticut 06520, USA. <sup>23</sup>Old Dominion University, Norfolk, Virginia 23529, USA. <sup>24</sup>Shanghai Institute of Applied Physics, Shanghai 201800, China. <sup>25</sup>Texas A&M University, College Station, Texas 77843, USA. <sup>26</sup>Variable Energy Cyclotron Centre, Kolkata 700064, India. <sup>27</sup>University of Science & Technology of China, Hefei 230026, China. <sup>28</sup>Institute of Particle Physics, CCNU (HZNU), Wuhan 400079, China. <sup>29</sup>Tsinghua University, Beijing 100084. China. <sup>30</sup>Craighton University, Omaha China. <sup>29</sup>Tsinghua University, Beijing 100084, China. <sup>30</sup>Creighton University, Omaha, Nebraska 68178, USA. 31 Pusan National University, Pusan 609-735, South Korea. <sup>32</sup>University of California, Berkeley, California 94720, USA. <sup>33</sup>University of Texas, Austin, Texas 78712, USA. <sup>34</sup>Institute of High Energy Physics, Protvino 142281, Russia. <sup>35</sup>Universidade Estadual de Campinas, Sao Paulo 13083-859, Brazil. <sup>36</sup>Wayne State University, Detroit, Michigan 48201, USA. <sup>37</sup>Rice University, Houston, Texas 77251, USA. <sup>38</sup>Pennsylvania State University, University Park, Pennsylvania 16802, USA. <sup>39</sup>University of Kentucky, Lexington, Kentucky, 40506-0055, USA. <sup>40</sup>Valparaiso University, Valparaiso, Indiana 46383, USA. <sup>41</sup>Purdue University, West Lafayette, Indiana 47907, USA. <sup>42</sup>Indiana University, Bloomington, Indiana 47408, USA. <sup>43</sup>Institute of Physics, Bhubaneswar 751005, India. 44Warsaw University of Technology, Warsaw 00-661, Poland. 45University of Frankfurt, Frankfurt 60325, Germany. 46Shandong University, Jinan, Shandong 250100, China. <sup>47</sup>Universidade de Sao Paulo, Sao Paulo 05508-090, Brazil. <sup>48</sup>University of Z30100, China. "Oniversidade de Sao Paulo, Sao Paulio USSUS-USU, Srazii. "University of Zagreb, HR-10002, Croatia. <sup>49</sup>Institute of Modern Physics, Lanzhou 730000, China. <sup>50</sup>University of Rajasthan, Jaipur 302004, India. <sup>51</sup>Max-Planck-Institut für Physik, Munich 80805, Germany. <sup>52</sup>Michigan State University, East Lansing, Michigan 48824, USA. <sup>53</sup>United States Naval Academy, Annapolis, Maryland 21402, USA.

# **CORRECTIONS & AMENDMENTS**

### **ERRATUM**

doi:10.1038/nature10264

### Observation of the antimatter helium-4 nucleus

The STAR Collaboration

Nature 473, 353-356 (2011)

In Fig. 2 of this Letter, the lower part of the figure was printed wrongly (the corrected Fig. 2 appears below). The online HTML and PDF versions are correct.

